

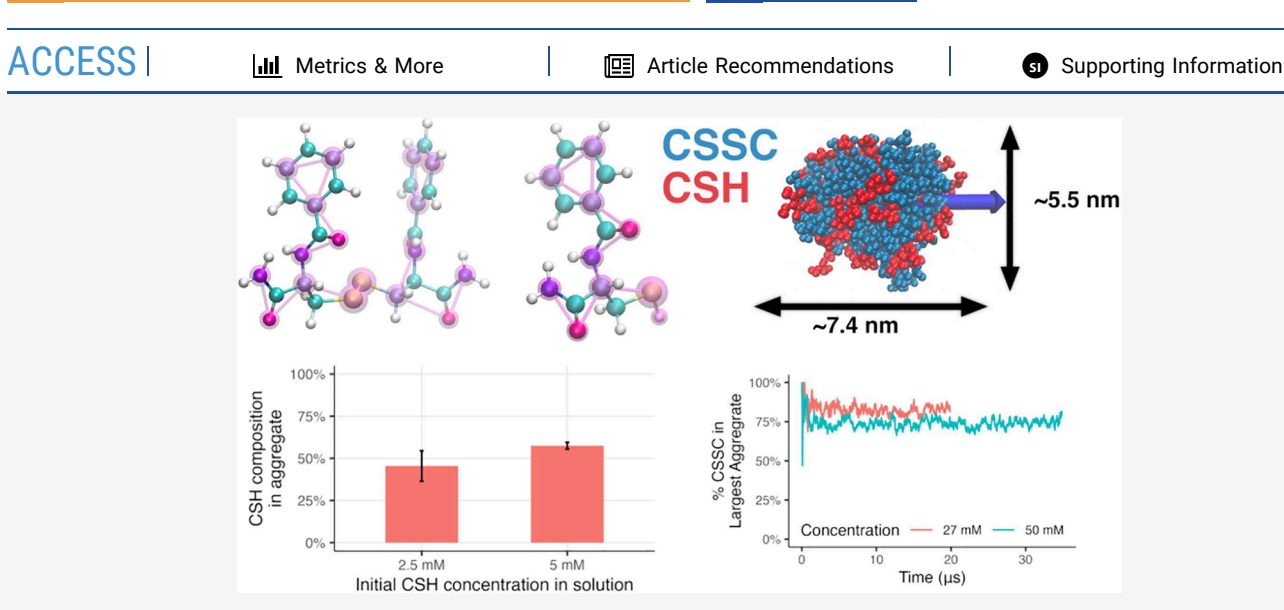
pubs.acs.org/JPCB Article

Multiscale Molecular Dynamics Simulations of an Active Self-Assembling Material

Published as part of The Journal of Physical Chemistry B virtual special issue "Gregory A. Voth Festschrift". Yuanming Song, Serxho Selmani, J. Alfredo Freites, Zhibin Guan, and Douglas J. Tobias*







ABSTRACT: Inspired by the adaptability observed in biological materials, self-assembly processes have attracted significant interest for their potential to yield novel materials with unique properties. However, experimental methods have often fallen short in capturing the molecular details of the assembly process. In this study, we employ a multiscale molecular dynamics simulation approach, complemented by NMR quantification, to investigate the mechanism of self-assembly in a redox-fueled bioinspired system. Contrary to conventional assumptions, we have uncovered a significant role played by the monomer precursor in the assembly process, with its presence varying with concentration and the extent of conversion of the monomer to the dimer. Experimental confirmation through NMR quantification underscores the concentration-dependent incorporation of monomers into the fibrous structures. Furthermore, our simulations also shed light on the diverse intermolecular interactions, including T-shaped and parallel π stacking, as well as hydrogen bonds, in stabilizing the aggregates. Overall, the open conformation of the dimer is preferred within these aggregates. However, inside the aggregates, the distribution of conformations shifts slightly to the closed conformation compared to on the surface. These findings contribute to the growing field of bioinspired materials science by providing valuable mechanistic and structural insights to guide the design and development of self-assembling materials with biomimetic functionalities.

INTRODUCTION

Molecular self-assembly is used for the creation of nanostructures and material properties through the organization of molecular building blocks exhibiting the appropriate intra- and intermolecular interactions to yield the desired structural and functional outcomes. Active self-assembly of materials has gained attention in recent years due to its potential applications in various fields, as it allows for the production of materials with tailored properties and performance. Many bioinspired small organic molecules, peptides, proteins, and nucleic acids that self-assemble have been used in a variety of applications such as the synthesis of conductive nanoma-

terials, drug delivery, and tumor diagnostics.^{2–5} CSH, an arylcontaining cysteine-based thiol that on its own does not self-assemble, when oxidized into its disulfide dimer (CSSC), becomes a hydrogelator capable of forming fibers.^{6–8} By using a redox reaction network to create and destroy the hydro-

Received: October 2, 2023 Revised: January 8, 2024 Accepted: January 9, 2024 Published: January 30, 2024





Table 1. Summary of CSSC-CSH Simulations Performed

concentration (mM)	box size (Å)	no. of waters	no. of CSHs	no. of CSSCs	conversion to CSSC (%)	simulation type	time (μs)
50	98	31434	32	0	0	atomistic	0.51
50	98	31469	24	4	25	atomistic	2.14
50	98	31432	16	8	50	atomistic	2.09
50	98	31483	8	12	75	atomistic	2.18
50	98	31500	0	16	100	atomistic	0.41
27	260	596420	161	80	50	CG	22.69
50	220	317053	321	0	0	CG	9.01
50	220	319198	161	80	50	CG	40.00
50	220	320947	0	160	100	CG	10.05

gelator, this self-assembly system can have transient dynamic behavior that depends on the reaction conditions and acts as an active self-assembly material. The emergent properties and the self-assembly process of the fibers can be further controlled both spatially and temporally by adjusting electrical signals on microelectrodes. However, previous studies did not investigate the molecular-level mechanistic or structural details of the fiber self-assembly, which are necessary for both understanding the self-assembly process and designing new self-assembling molecules.

Hydrogen bonding has long been recognized as a crucial intermolecular force driving the aggregation of gelators like CSSC. 10 Additionally, van der Waals interactions, coupled with the unique space-filling properties of nonpolar side chains, have been postulated to offer selective binding sites for fiber growth. Trystal structures of di(p-toluoyl)-L-cystine (DTC), differing from CSSC through two aromatic methyl substitutions and two carboxyl groups, exhibit various modes of molecular packing. The first mode involves aromatic amide moieties forming hydrogen bonds with carboxyl groups from neighboring molecules, resulting in a backbone arrangement that aligns all aromatic groups in parallel, resembling a DNAlike structure. In the second mode, a similar backbone hydrogen bonding configuration is observed but with the aromatic rings oriented in distinct directions.7 Crystal structures of di(p-nitrobenzoyl)-L-cystine (DNC), differing from DTC through two aromatic nitro substitutions, showcase a third mode. In this arrangement, each gelator adopts an open conformation, with two aromatic groups distantly positioned away from each other. Nonetheless, these groups stack in parallel with neighboring gelators, stabilized by intermolecular hydrogen bonds between neighboring amide protons and carboxyl oxygens. NMR results from bis(phenylalanine) oxalyl amides, distinct from CSSC due to an oxalyl amide backbone and aromatic carboxyl groups, suggest a fourth possible packing mode. This mode gives rise to a lipid bilayer-like structure, wherein phenyl groups are closely packed in the central region, while the backbones are exposed to the solvent. 11 Furthermore, crystal structures of naphthalenedipeptides reveal additional modes of aromatic ring stacking, encompassing off-centered parallel stacking and displaced edge-to-faceinteractions between phenyl groups. 12

Although the analysis of crystal structures offers some valuable insights into the macroscopic properties of gels, it is often insufficient in elucidating the dynamic interactions within the gel matrix.^{7,12} Molecular dynamics (MD) simulations have emerged as powerful tools for studying the self-assembly processes of various systems, including small molecules, peptides, and proteins. Fully atomistic MD simulations have provided insights into the intricate molecular interactions that

govern the self-assembly of these systems. ^{13–15} However, due to their high computational cost, atomistic MD simulations are not a suitable approach when exploring self-assembly processes at larger length and time scales.

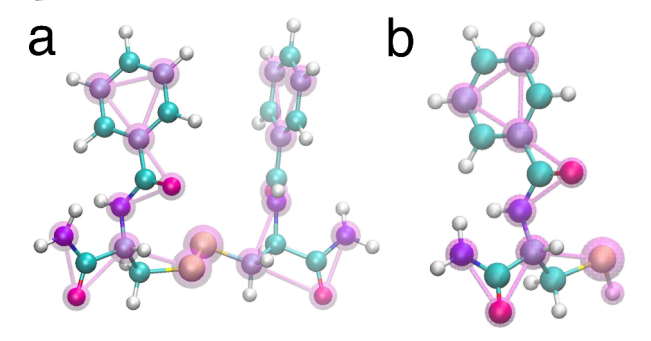
To overcome these limitations, coarse-grained (CG) MD simulations have been developed to offer a more computationally efficient approach for studying self-assembly phenomena. 16 By simplifying the extraneous details in molecular representations, CG simulations offer a cost-effective approach to capture the fundamental aspects of self-assembly. 16 CG simulations routinely enable tens of microsecond-time scale simulations of systems containing thousands of self-assembling small molecules, as opposed to fully atomistic simulations, which are typically limited to nanosecond-microsecond time scales and hundreds of small molecules. 16 This enhanced capability is essential to study extensive and prolonged selfassembly behavior of biomolecules and functional materials, facilitating a deeper understanding of these complex systems. However, as CG models sacrifice some atomiclevel information, a challenge is to capture faithfully the precise structural arrangements and fine-grained dynamics of the assembled systems. Therefore, the interpretation of CG simulation results should be done with validation with fully atomistic simulation.¹⁶ Through both fully atomistic and CG simulations, fundamental mechanisms of self-assembly can be understood, and new materials with tailored properties can be designed and synthesized. 18,19 However, existing simulation studies on self-assembling systems predominantly operate within densely populated environments rather than reflecting concentrations consistent with experimental conditions.²⁰⁻ Additionally, these investigations often overlook the significant role played by precursors, a crucial factor in understanding active self-assembly systems. 20-23

Here, we follow a multiscale MD simulation approach that utilizes both fully atomistic and CG simulations to investigate the self-assembly of the CSH/CSSC system. We find that CSSC readily aggregates in solution and free CSH can participate in these aggregates in a concentration dependent manner. The concentration dependent presence of CSH in self-assembled fibers was verified using solution $^1\mathrm{H}$ NMR. We find that hydrogen bonding between amide N–H and carbonyl oxygen as well as both parallel and T-shaped $\pi-\pi$ interactions is involved in aggregate stabilization. Aggregate growth appears to be modulated by transitions from open to closed conformations of CSSC molecules upon their integration into the aggregates.

METHODS

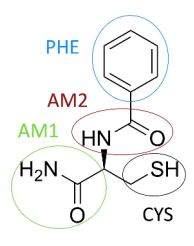
Atomistic Simulations. Five all-atom MD simulations were prepared, each comprising 32 CSH-equivalent units, with

Scheme 1. Illustration of the Coarse-Grained Bead Mapping (Magenta) Depicting (a) CSSC and (b) CSH Molecules, Derived from Their Corresponding Fully Atomistic Representation^a



^aC: cyan. O: red. N: blue. H: white. S: yellow.

Scheme 2. Illustration of Moiety Definition for Graph Representation of CSH: Phenyl Ring (PHE), Terminal Amide (AM1), Aromatic Amide (AM2), and Thiol (CYS)



varying extents of dimerization (0%, 25%, 50%, 75%, and 100%) at a concentration of 50 mM (Table 1). The corresponding CSH and CSSC molecules were positioned in a cubic grid and solvated in 250 mM NaCl aqueous solutions. System preparation was performed using the VMD 1.9.3 software package.²⁴

All-atom MD simulations were performed using NAMD3a6 and NAMD3a11. 25,26 The CSH force field parameters were generated using the CHARMM general force field (CGenFF) program version 1.0.0 with the CGenFF force field version 2.4.0.²⁷⁻³⁰ CSSC was modeled by using the disulfide bond patch from the CHARMM36m protein force field to connect two CSH molecules. 31,32 The TIP3P model³³ was used for water, and the CHARMM36 force field³¹ was used for the ions. The initial configuration was subjected to 10 000 steps of conjugate gradient energy minimization, followed by a 250 ps MD simulation during which harmonic restraints on the heavy atoms of CSSC and/or CSH were gradually relaxed. The smooth particle-mesh Ewald method^{34,35} was used to calculate the electrostatic interactions. Short-range, real-space interactions were cut off at 10 Å by means of a switching function. A reversible, multiple time-step algorithm was used to integrate the equations of motion with a time step of 4 fs for electrostatic forces, 2 fs for short-range nonbonded forces, and 1 fs for bonded forces.³⁶ The SHAKE and SETTLE algorithms were used to hold fixed all covalent bonds involving hydrogen.^{37,38} The simulations were run at constant temperature (300 K) and constant pressure (1 bar). A Langevin dynamics scheme was used for temperature control, and a Nosé-Hoover-Langevin piston was used for pressure control. 39,40

Coarse-Grained Simulations. Four CG simulation systems with 321 CSH-equivalent units were prepared, three

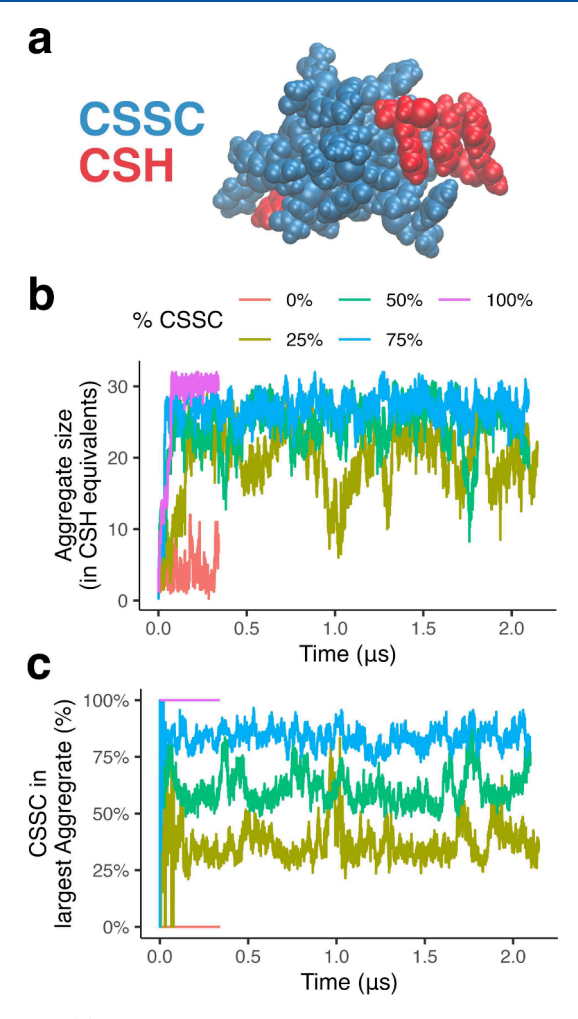


Figure 1. (a) Configuration snapshot of the largest aggregate in the 32-unit fully atomistic simulation at 50 mM and 50% conversion to CSSC. Time evolution of (b) aggregate size (in number of CSH equivalents) and (c) the percentage of CSSC in the largest aggregates. The presence of CSSC leads to aggregation, and both CSH and CSSC are present in the aggregates. In all simulations, almost all CSSC are in the largest aggregates.

systems at a concentration 50 mM and varying dimerization extent (0%, 50%, and 100%) and one at a concentration of 27 mM and 50% conversion to CSSC (Table 1). Coarse-grained models of CSH and CSSC were generated from all-atom representations using the SIRAH 2.0 mapping for proteins as shown in Scheme 1.41 The corresponding number of CG molecules were placed on a grid using VMD 1.9.3 and solvated in 250 mM aqueous NaCl using GROMACS 2020.4.24,42,43

The CG MD simulations were performed using the GROMACS software package (versions 2020.4 and 2022.1). 42,43 The SIRAH 2.0 force field for proteins was used for CSH and CSSC,41 and the WT4 model was used for waters with the corresponding SIRAH models for ions.⁴⁴ The initial configuration was subjected to 45 000 steps of steepest descent energy minimization, followed by a 1.5 ns of dynamics over which positional restraints of 1000 kJ·mol⁻¹·nm⁻² were applied on all CSH and/or CSSC CG beads. The smooth particle-mesh Ewald method was used to calculate electrostatic interactions. 34,35 Short-range, real-space interactions were cut off at 12 Å by means of a switching function. The leap-frog integrator was used to integrate the equations of motion with a time step of 20 fs. 45 The simulations were run at constant

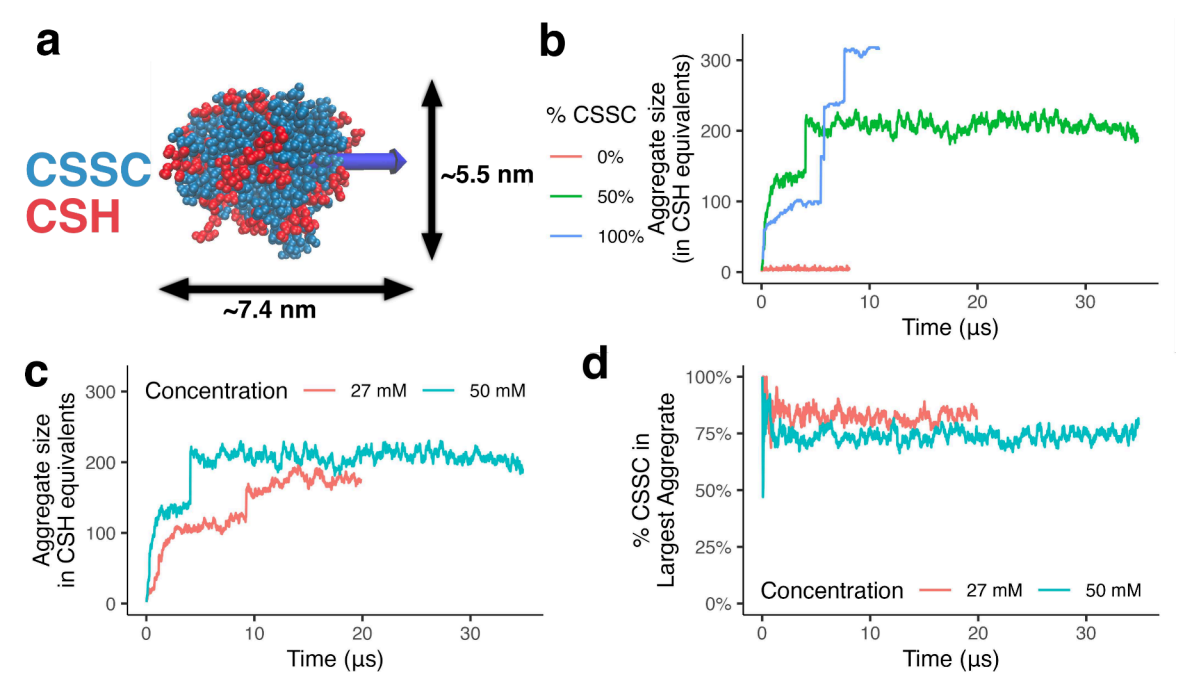


Figure 2. (a) Configuration snapshot of the largest aggregate, with main principal axis drawn in blue, formed in the 321-unit CG simulation at 50 mM with 50% conversion to CSSC. Time evolution of the size of the largest aggregate (in CSH equivalents) (b) at 50 mM with different percent conversion to CSSC and (c) at two different concentrations with 50% conversion to CSSC and (d) percentage of CSSC in the largest aggregate at 50% conversion to CSSC. In all simulations, almost all CSSCs are in the largest aggregates.

temperature (300 K) and constant pressure (1 bar), with the V-rescale thermostat for temperature control and the Parrinello–Rahman barostat for pressure control. 46,47

Simulation Analysis. CSSC-CSH aggregates were identified and characterized using a graph representation, wherein vertices correspond to small molecular moieties as shown in Scheme 2: phenyl ring (PHE), terminal amide (AM1), aromatic amide (AM2) and thiol (CYS), and edges are assigned if any two heavy atoms (in the atomistic systems) or beads (in the coarse-grained systems) are found at a distance of less than a cutoff value (atomistic systems, 5.4 Å, for carbon—carbon, 6.3 Å for sulfur—sulfur, and 4.6 for all other pairs; coarse-grained systems, 5 Å for all pairs). Graph representations were generated using VMD 1.9.3, and network analyses were performed using the Social Network Analysis (SNA) package for the R statistical computing environment. Molecular graphics were generated with VMD. Molecular graphics were generated with VMD.

NMR Quantification of Fiber Composition. Fibers were prepared as previously described. Secretary, solutions of 2.5 and 5 mM CSH in pH 6 Tris buffer were prepared in 1 mL microcentrifuge vials, to which an appropriate quantity of hydrogen peroxide was added to achieve 50% conversion of CSH to CSSC. The samples were vortexed thoroughly to mix, followed by an incubation period of 1.5 h to allow the reaction to reach completion resulting in full gelation of the system. The vials were centrifuged at 800 rcf for 30 min to separate the gel phase from the supernatant. A sample was collected and dissolved in DMSO- d_6 for 1 H NMR analysis.

 ^1H NMR measurements were conducted to probe the composition of the gel phase, employing an average of both the benzamide proton (δ 4.52 ppm for CSH, 4.73 ppm for CSSC) and methine proton peaks (δ 8.49 ppm for CSH, 8.63 ppm for CSSC) of CSH and CSSC. These peaks were fully resolved and chosen for their suitability in gauging the relative

quantities of CSH and CSSC present within the gel phase. A representative ¹H NMR spectrum for the gel sample is included in the Supporting Information (Figure S3).

■ RESULTS AND DISCUSSION

Motivated by the goal of characterizing the molecular interactions that control the self-assembly of CSH and CSSC

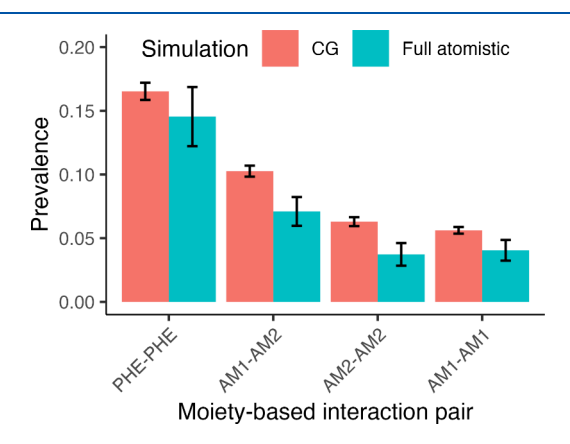


Figure 3. Prevalence of pairwise moiety-based interactions in the largest aggregate at 50 mM and 50% conversion to CSSC. Comparable values for key interactions suggest consistency between the fully atomistic and CG MD simulations.

into fibers, the aim of this study is to elucidate the fundamental processes governing the aggregation behavior through multiscale MD simulations. Fully atomistic simulations of CSH/CSSC in solution were performed with various CSH:CSSC ratios and concentrations, with additional CG simulations conducted to explore larger aggregates (Table 1).

The atomistic simulations show that CSSC readily aggregates in solution (Figure 1), consistent with the available

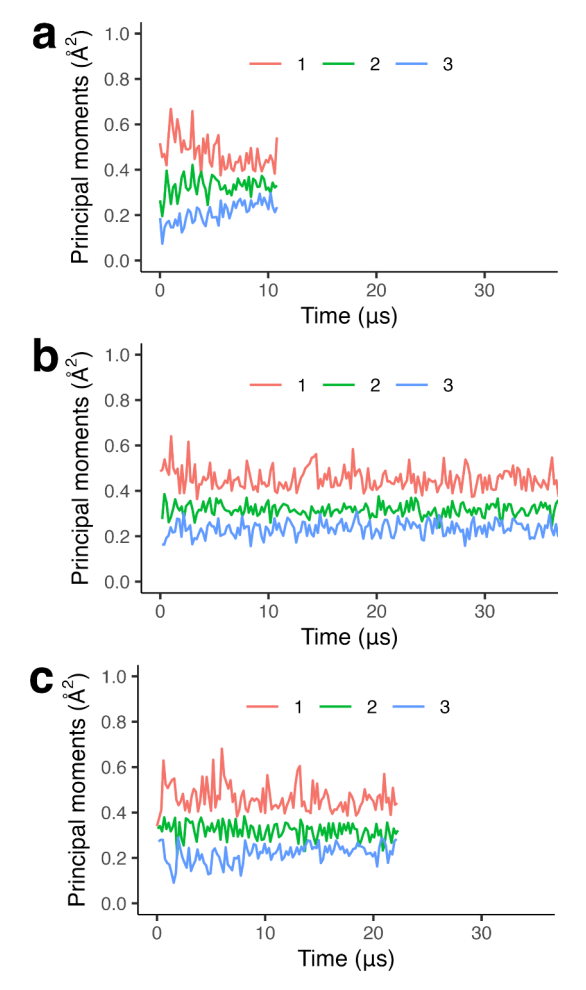


Figure 4. Time evolution of gyration tensor moments of the largest aggregate in the 321 CSH-equivalent unit CG simulations (a) at 50 mM with 100% conversion to CSSC, (b) at 50 mM with 50% conversion to CSSC (see Figure 2), and (c) at 27 mM with 50% conversion to CSSC.

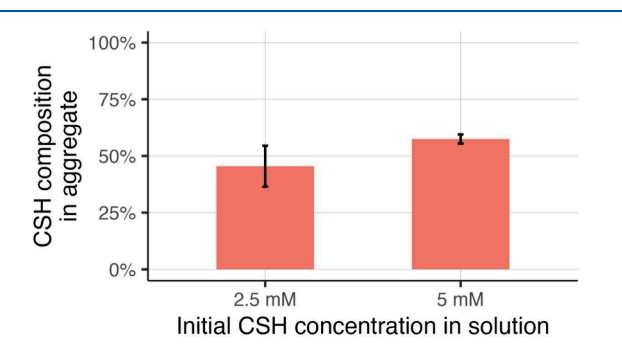


Figure 5. Average percentage of CSH in fibers from liquid-phase ¹H NMR determined by both amide proton and methylene proton peaks. The presence of CSH is concentration dependent and qualitatively agrees with the MD simulations (see Figure 1c and Figure 2d).

experimental evidence.⁷ As shown in Figure 1b, higher conversion to CSSC leads to larger and more stable aggregates. While the pure CSH system also had some small aggregates, they disassembled rapidly. Further analysis of the makeup of the aggregates (Figure 1c) reveals that CSH participates in the aggregation, which was not considered in previous experimental studies.^{6–8}

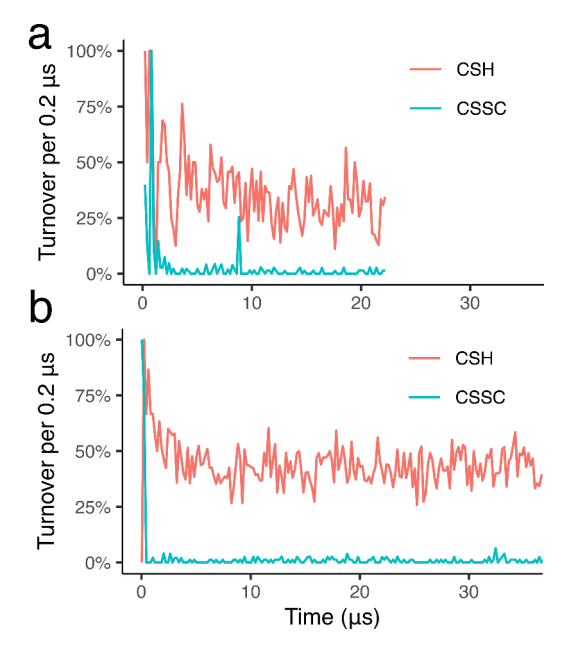


Figure 6. Individual molecule turnover every 0.2 μ s in CSH/CSSC aggregates in 321-unit CG simulations with 50% conversion to CSSC at (a) 27 mM and (b) 50 mM. While both engage in aggregation, CSSC is more stable within the aggregates than CSH.

To verify that the aggregation observed in the 32 CSH-equivalent units atomistic simulations was not an artifact of the small system size, we performed CG simulations of 321 CSH-equivalent units at 50 mM in solution (Figure 1). As shown in Figure 2b, the larger CG simulation system exhibits aggregation behavior similar to that observed in the atomistic simulations and confirms that aggregation is strictly due to the presence of CSSC. However, even at the CG-level, it is not feasible to perform simulations at the CSH concentration levels of 10 mM used in experiments. Nevertheless, Figure 2c,d demonstrates that aggregation still occurs in a similar manner at the lower concentration of 27 mM.

Figure 3 shows that, at a 50 mM concentration of CSH-equivalent units and 50% conversion to CSSC, the prevalence of key moiety-based interactions that are involved in the CSH/CSSC self-assembly^{7,23} are similar in the CG and atomistic simulations. This consistency between both levels of molecular representation confirms that the SIRAH CG model is suitable for scaling-up MD simulations of CSH-CSSC systems.

CSH in solution self-assembles into fibers upon oxidation to CSSC. 8,52 Although the 321 CSH-equivalent CG simulations are too small to generate fibers, an analysis of the largest aggregate gyration tensor shows persistent anisotropy across all simulations, as shown in Figure 4. These results suggests that fiber growth may be achieved in a hierarchical manner via the coalescence of anisotropic aggregates such as the one depicted in Figure 2a.

Our simulations show consistent participation of CSH in the aggregation of the CSSC/CSH systems in a concentration-dependent manner and predict that the higher the CSH concentration, the more CSH is involved in the largest aggregate. To verify this prediction, we performed NMR analysis of the fibers obtained from experiments in which the conversion of CSH to CSSC was 50%. As shown in Figure 5 and Tables S1 and S2, CSH is present in a similar concentration dependent manner in fibers produced upon incomplete conversion of CSH to CSSC. While CSH and

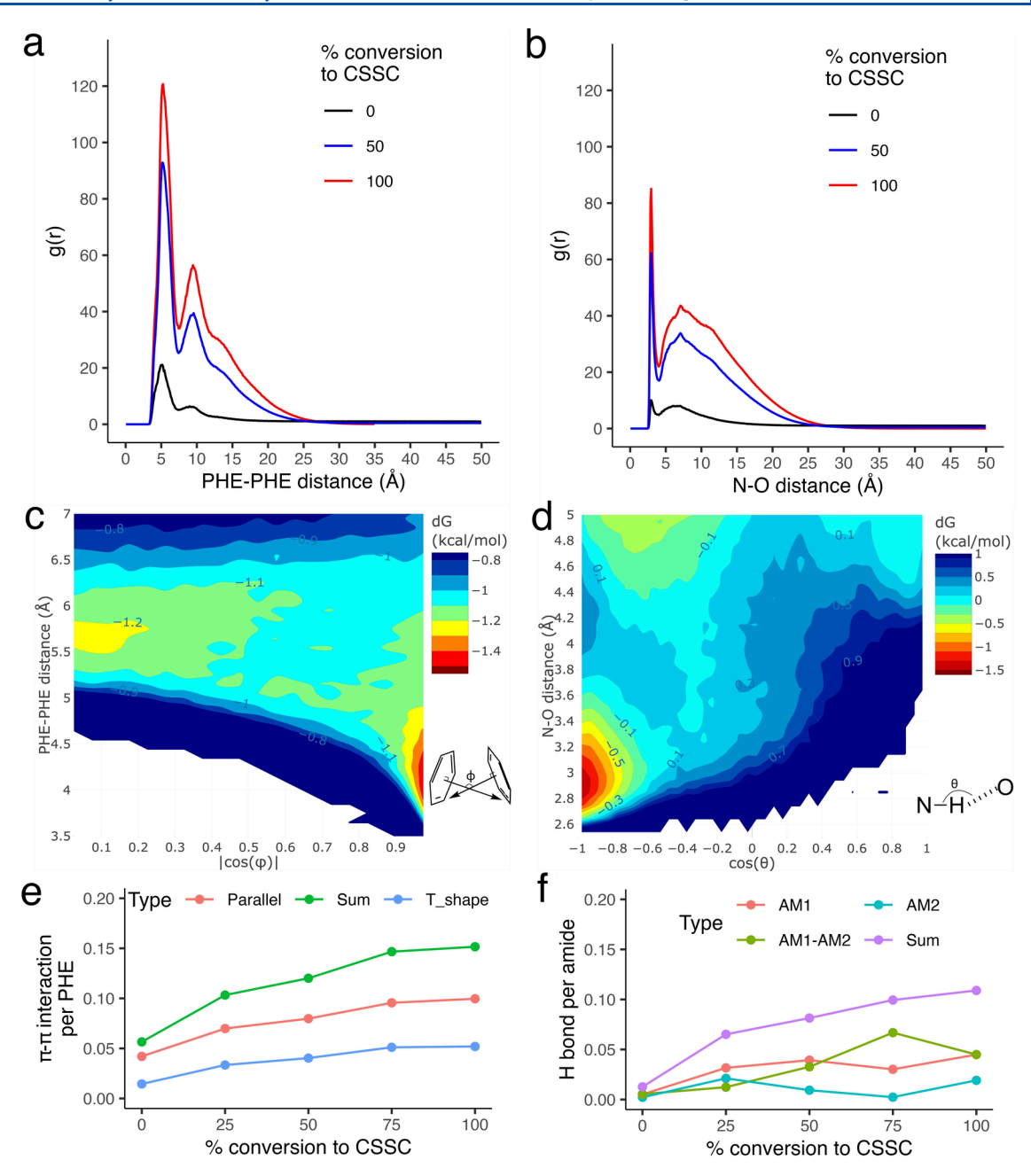


Figure 7. Intermolecular radial distribution functions of (a) the center-of-mass distance between phenyl (PHE) rings and (b) oxygen to nitrogen distance between amide groups. Two-dimensional distributions (expressed as free energies) of (c) the distance between PHE rings and angle between normal vectors to the rings in PHE-PHE intermolecular pairs, and of (d) the distance between oxygen and nitrogen and O···N-H angle in amide-amide intermolecular pairs, at 100% CSSC conversion. (e) π - π interactions (as defined in the text) per PHE group (Scheme 2), and (f) hydrogen-bond configurations (as defined in the text) per amide group (Scheme 2) as functions of percent conversion to CSSC. All data are obtained from atomistic simulations.

CSSC both engage in aggregation, their stability in the aggregates differs vastly as shown by their turnover in the aggregate, defined as the percentage of molecules of interest that are no longer in the aggregate from the previous time lag of $0.2 \ \mu s$ in the MD simulations (Figure 6).

Both intermolecular hydrogen bonding and $\pi-\pi$ interactions have been identified in the experimental literature as participating in the self-assembly of small hydrogelators, such as CSH/CSSC.^{6,7,11,12} To characterize these interactions in our atomistic simulations, we analyzed the relevant configurational landscapes as shown in Figure 7a–d. The distance—angle

histograms shown in Figure 7c and Figure 7d are expressed in free-energy units according to

$$\delta G = -k_{\rm B} T \log \left(\frac{P(r, \cos(\theta))}{P_{\rm ref}} \right)$$
 (1)

where $k_{\rm B}$ is Boltzmann's constant and $P(r,\cos(\theta))$ is the distance—angle joint probability density. The reference state, with density $P_{\rm re\theta}$ was taken as the average at a distance of 35 Å for all angles.

T-shaped and parallel $\pi - \pi$ interactions are defined as distance-angle pairs within the $\delta G = -1.2 \text{ kcal·mol}^{-1}$ contours

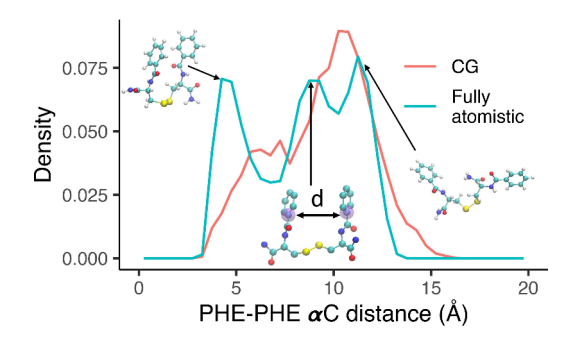


Figure 8. PHE–PHE intramolecular distance probability density, measured as the distance (d) between the phenyl carbons linked to the carbonyl carbon (α C), for a single CSSC molecule in solution. Snapshots corresponding to selected α C distances are included.

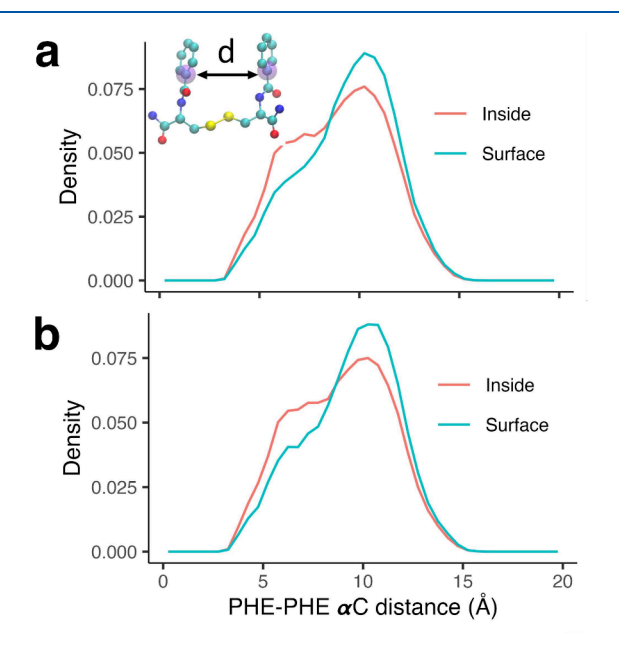


Figure 9. PHE–PHE intramolecular distance probability density, measured as the distance (d) between the phenyl carbons linked to the carbonyl carbon (α C), in the largest aggregate in the CG simulations at (a) 100% CSSC conversion and (b) 50% CSSC conversion.

in the PHE–PHE distance-angle histogram (Figure 7c). Hydrogen bonds are defined as when acceptor O and donor N are within 3.5 Å and the acceptor—hydrogen—donor angle is larger than 147° (Figure 7d). Figure 7e,f shows that both interactions are enhanced with increased percent conversion to CSSC, which suggest both are important to aggregate stability. Notably, crystal structures formed by molecules similar to CSSC predominantly exhibit intermolecular hydrogen bonds between the aromatic amide (AM1) group and nonaromatic carboxylic groups (AM2 equivalent). 7,11,12 However, in our simulations, an equal number of intermolecular hydrogen bonds occur between the two aromatic amide groups as well as between an aromatic amide (AM1) group and a nonaromatic amide.

The distribution of the distance between the phenyl carbons linked to the carbonyl carbon (α C) in the two PHE groups in an individual CSSC was computed to investigate the conformational preferences of CSSC. At infinite dilution, both open (higher distances) and closed (lower distances) conformations are present in both the atomistic and CG

simulations, but in the CG simulation the open conformation is more preferred (Figure 8). Figure 9 shows that in the CG simulation, when CSSC has one or more aromatic rings exposed to solvent on the surface of aggregates, it shifts to a more open configuration than the CSSC inside the aggregates. An in-depth analysis of the dihedral angle in PHE-S-S-PHE indicates no specific preference for the relative ring position at PHE-PHE an increased distance (Figure S2).

X-ray crystallographic structures of compounds that are structurally similar to CSSC have revealed that both open and closed conformations could form fibrilar assemblies stabilized by hydrogen bonding, and structures of aromatic-rich dipeptides have shown that off-centered parallel and T-shaped $\pi - \pi$ interactions are possible stabilizing forces within aggregates. 6,7,11,12 Specifically, when compared to the parent compound of CSSC, dibenzyl-L-cystine, and its derivative, di(p-toluoyl)-L-cystine, the presence of the amide groups in CSSC, in place of the carboxyl groups, potentially reduces the likelihood of selective intermolecular hydrogen bonding between amide and carboxyl groups. 6,7 Consequently, there is a higher propensity for hydrogen bonding of CSSC with water, thereby favoring gelation over crystallization. Additionally, the diminished selective hydrogen bonding might also confer greater conformational flexibility to the CSSC molecules. This increased flexibility could facilitate the close packing of CSSC molecules assuming closed conformations deep inside the aggregates, while concomittantly allowing for hydrogen bonding with water in more open conformations on the surface of the aggregates.

CONCLUSIONS

The present study utilized atomistic and CG MD simulations to investigate the aggregation behavior of the CSH/CSSC system. The simulations demonstrated that when conversion to CSSC is not 100%, both CSH and CSSC are present in the fibers, in contrast to previous assumptions that only CSSC is involved. Furthermore, the higher the concentration of CSH and CSSC, the more CSH is present in the aggregates, as confirmed by NMR results reported here. Interestingly, CSH is less stable in aggregates compared to CSSC, suggesting that CSSC may act as a nucleation site for CSH.

Examination of the importance of intermolecular forces in the formation of aggregates also revealed that both $\pi-\pi$ interactions and hydrogen bonding play significant roles. Additionally, our simulations showed that while CSSC molecules overall have a more open configuration, CSSC molecules inside the aggregates tend to adopt a closed configuration more frequently compared to those on the surface, possibly allowing them to interlock with one another through their phenyl rings. Disulfide bonds were found to potentially stabilize the open configuration of CSSC, thus promoting initial nucleation via $\pi-\pi$ interactions on the surface of the nascent clusters.

Overall, this study highlights the importance of considering the participation of CSH in the formation of CSH-CSSC aggregates and provides new insights into the underlying mechanisms governing their assembly and the interactions determining their stability. These findings may have implications for the design of novel materials with tunable self-assembly properties.

ASSOCIATED CONTENT

Supporting Information

The Supporting Information is available free of charge at https://pubs.acs.org/doi/10.1021/acs.jpcb.3c06572.

Two-dimensional distributions of PHE–S–S–PHE dihedral angle and PHE–PHE distance in atomistic and CG simulations; two-dimensional distribution of the distance between PHE rings and the angle between normal vectors to the rings in PHE–PHE intermolecular pairs, with snapshot of selective π – π orientation; representative ¹H NMR spectrum for the fiber gel sample; tabulated NMR results for CSH composition in fibers at 50% conversion to CSSC (PDF)

AUTHOR INFORMATION

Corresponding Author

Douglas J. Tobias — Department of Chemistry, University of California, Irvine, Irvine, California 92697, United States; Center for Complex and Active Materials, University of California, Irvine, Irvine, California 92697, United States; orcid.org/0000-0002-6971-9828; Email: dtobias@uci.edu

Authors

Yuanming Song – Department of Chemistry, University of California, Irvine, Irvine, California 92697, United States; Center for Complex and Active Materials, University of California, Irvine, Irvine, California 92697, United States

Serxho Selmani – Department of Chemistry, University of California, Irvine, Irvine, California 92697, United States; Center for Complex and Active Materials, University of California, Irvine, Irvine, California 92697, United States

J. Alfredo Freites – Department of Chemistry, University of California, Irvine, Irvine, California 92697, United States; orcid.org/0000-0001-5842-7443

Zhibin Guan — Department of Chemistry, University of California, Irvine, Irvine, California 92697, United States; Center for Complex and Active Materials, University of California, Irvine, Irvine, California 92697, United States; orcid.org/0000-0003-1370-1511

Complete contact information is available at: https://pubs.acs.org/10.1021/acs.jpcb.3c06572

Notes

The authors declare no competing financial interest.

ACKNOWLEDGMENTS

This work was supported by National Science Foundation Materials Research Science and Engineering Center program through the UC Irvine Center for Complex and Active Materials (Grant DMR-2011967, Z.G. and D.J.T.), the National Science Foundation (Grant CHE-1904939, Z.G.), and the U.S. Department of Energy, Office of Science, Basic Energy Sciences (Grant DE-FG02-04ER46162, Z.G.)

REFERENCES

- (1) Pochan, D.; Scherman, O. Introduction: Molecular Self-Assembly. Chem. Rev. 2021, 121, 13699-13700.
- (2) Lin, Y.; Mao, C. Bio-inspired supramolecular self-assembly towards soft nanomaterials. *Front. Mater. Sci.* **2011**, *5*, 247–265.

- (3) Ing, N. L.; Spencer, R. K.; Luong, S. H.; Nguyen, H. D.; Hochbaum, A. I. Electronic Conductivity in Biomimetic α-Helical Peptide Nanofibers and Gels. *ACS Nano* **2018**, *12*, 2652–2661.
- (4) Zhao, Y.; Li, X.; Zhao, X.; Yang, Y.; Li, H.; Zhou, X.; Yuan, W. Asymmetrical Polymer Vesicles for Drug delivery and Other Applications. *Front. Pharmacol.* **2017**, *8*, 2652–2661.
- (\$\tilde{s}\$) Ren, Z.; Sun, S.; Sun, R.; Cui, G.; Hong, L.; Rao, B.; Li, A.; Yu, Z.; Kan, Q.; Mao, Z. A Metal—Polyphenol-Coordinated Nanomedicine for Synergistic Cascade Cancer Chemotherapy and Chemodynamic Therapy. *Adv. Mater.* **2020**, *32*, 1906024.
- (6) Menger, F. M.; Yamasaki, Y.; Catlin, K. K.; Nishimi, T. X-Ray Structure of a Self-Assembled Gelating Fiber. *Angew. Chem., Int. Ed. Engl.* **1995**, 34, 585–586.
- (7) Menger, F. M.; Caran, K. L. Anatomy of a Gel. Amino Acid Derivatives That Rigidify Water at Submillimolar Concentrations. *J. Am. Chem. Soc.* **2000**, *122*, 11679–11691.
- (8) Ogden, W. A.; Guan, Z. Redox Chemical-Fueled Dissipative Self-Assembly of Active Materials. *ChemSystemsChem* **2020**, *2*, e1900030.
- (9) Selmani, S.; Schwartz, E.; Mulvey, J. T.; Wei, H.; Grosvirt-Dramen, A.; Gibson, W.; Hochbaum, A. I.; Patterson, J. P.; Ragan, R.; Guan, Z. Electrically Fueled Active Supramolecular Materials. *J. Am. Chem. Soc.* **2022**, *144*, 7844–7851.
- (10) Kölbel, M.; Menger, F. M. Molecular Recognition among Structurally Similar Components of a Self-Assembling Soft Material. *Langmuir* **2001**, *17*, 4490–4492.
- (11) Makarević, J.; Jokić, M.; Perić, B.; Tomišić, V.; Kojić-Prodić, B.; Žinić, M. Bis(Amino Acid) Oxalyl Amides as Ambidextrous Gelators of Water and Organic Solvents: Supramolecular Gels with Temperature Dependent Assembly/Dissolution Equilibrium. *Chem.—Eur. J.* **2001**, *7*, 3328–3341.
- (12) Adams, D. J.; Morris, K.; Chen, L.; Serpell, L. C.; Bacsa, J.; Day, G. M. The delicate balance between gelation and crystallisation: structural and computational investigations. *Soft Matter* **2010**, *6*, 4144.
- (13) Ma, Y.; Wang, N.; Huang, X.; Wang, T.; Zhou, L.; Li, X.; Ji, X.; Zhao, Y.; Hao, H. Self-assembly process of organic small molecular gel and its molecular mechanism. *Particuology* **2023**, *72*, 122–133.
- (14) Divanach, P.; Fanouraki, E.; Mitraki, A.; Harmandaris, V.; Rissanou, A. N. Self-Assembly of Phenylalanine-Leucine, Leucine-Phenylalanine, and Cyclo(-leucine-phenylalanine) Dipeptides through Simulations and Experiments. *J. Phys. Chem. B* **2023**, *127*, 4208–4219
- (15) Bystrov, V.; Likhachev, I.; Filippov, S.; Paramonova, E. Molecular Dynamics Simulation of Self-Assembly Processes of Diphenylalanine Peptide Nanotubes and Determination of Their Chirality. *Nanomater.* **2023**, *13*, 1905.
- (16) Cranford, S.; Buehler, M. J. In *Multiscale Modeling*; Derosa, P., Cagin, T., Eds.; CRC Press: Boca Raton, FL, 2010; p 22.
- (17) Darré, L.; Machado, M. R.; Brandner, A. F.; González, H. C.; Ferreira, S.; Pantano, S. SIRAH: a structurally unbiased coarse-grained force field for proteins with aqueous solvation and long-range electrostatics. Journal of chemical theory and computation. *J. Chem. Theory Comput.* **2015**, *11*, 723–739.
- (18) Orsi, M. Self-Assembling Biomaterials; Elsevier, 2018; pp 305-318
- (19) Pirhadi, S.; Amani, A. Molecular dynamics simulation of self-assembly in a nanoemulsion system. *Chem. Pap.* **2020**, *74*, 2443–2448.
- (20) Williams-Noonan, B. J.; Kamboukos, A.; Todorova, N.; Yarovsky, I. Self-assembling peptide biomaterials: Insights from spontaneous and enhanced sampling molecular dynamics simulations. *Chem. Phys. Rev.* **2023**, *4*, 021304.
- (21) Zhang, G.; Yue, K.; Wang, A.; Zhong, W.; Yang, P.; Wang, L.; Ye, X.; Sun, X. Self-assembly and disassembly mechanisms of biomimetic peptides: Molecular dynamics simulation and experimental measurement. *Int. J. Biol. Macromol.* **2022**, 209, 785–793.
- (22) Frederix, P. W. J. M.; Patmanidis, I.; Marrink, S. J. Molecular simulations of self-assembling bio-inspired supramolecular systems and their connection to experiments. *Chem. Soc. Rev.* **2018**, 47, 3470—3489.

- (23) Aprahamian, I.; Goldup, S. M. Non-equilibrium Steady States in Catalysis, Molecular Motors, and Supramolecular Materials: Why Networks and Language Matter. *J. Am. Chem. Soc.* **2023**, *145*, 14169—14183.
- (24) Humphrey, W.; Dalke, A.; Schulten, K. VMD Visual Molecular Dynamics. *J. Mol. Graph.* **1996**, *14*, 33–38.
- (25) Phillips, J. C.; Braun, R.; Wang, W.; Gumbart, J.; Tajkhorshid, E.; Villa, E.; Chipot, C.; Skeel, R. D.; Kale, L. d.; Schulten, K. Scalable molecular dynamics with NAMD. *J. Comput. Chem.* **2005**, *26*, 1781–1802.
- (26) Phillips, J. C.; Hardy, D. J.; Maia, J. D. C.; Stone, J. E.; Ribeiro, J. V.; Bernardi, R. C.; Buch, R.; Fiorin, G.; Hénin, J.; Jiang, W.; et al. Scalable molecular dynamics on CPU and GPU architectures with NAMD. *J. Chem. Phys.* **2020**, *153*, 044130.
- (27) Vanommeslaeghe, K.; Hatcher, E.; Acharya, C.; Kundu, S.; Zhong, S.; Shim, J.; Darian, E.; Guvench, O.; Lopes, P.; Vorobyov, I.; Mackerell, A. D., Jr. CHARMM general force field: A force field for drug-like molecules compatible with the CHARMM all-atom additive biological force fields. *J. Comput. Chem.* **2010**, *31*, 671.
- (28) Yu, W.; He, X.; Vanommeslaeghe, K.; MacKerell, A. D. Extension of the CHARMM general force field to sulfonyl-containing compounds and its utility in biomolecular simulations. *J. Comput. Chem.* **2012**, *33*, 2451–2468.
- (29) Vanommeslaeghe, K.; MacKerell, A. D. Automation of the CHARMM General Force Field (CGenFF) I: Bond Perception and Atom Typing. *J. Chem. Inf. Model.* **2012**, *52*, 3144–3154.
- (30) Vanommeslaeghe, K.; Raman, E. P.; MacKerell, A. D. Automation of the CHARMM General Force Field (CGenFF) II: Assignment of Bonded Parameters and Partial Atomic Charges. *J. Chem. Inf. Model.* **2012**, *52*, 3155–3168.
- (31) Huang, J.; MacKerell, A. D. CHARMM36 all-atom additive protein force field: Validation based on comparison to NMR data. *J. Comput. Chem.* **2013**, 34, 2135–2145.
- (32) Huang, J.; Rauscher, S.; Nawrocki, G.; Ran, T.; Feig, M.; de Groot, B. L.; Grubmüller, H.; MacKerell, A. D. CHARMM36m: an improved force field for folded and intrinsically disordered proteins. *Nat. Methods* **2017**, *14*, 71–73.
- (33) Jorgensen, W. L.; Chandrasekhar, J.; Madura, J. D.; Impey, R. W.; Klein, M. L. Comparison of simple potential functions for simulating liquid water. *J. Chem. Phys.* **1983**, *79*, 926–935.
- (34) Darden, T.; York, D.; Pedersen, L. Particle mesh Ewald: An N·log(N) method for Ewald sums in large systems. *J. Chem. Phys.* **1993**, 98, 10089–10092.
- (35) Essmann, U.; Perera, L.; Berkowitz, M. L.; Darden, T.; Lee, H.; Pedersen, L. G. A smooth particle mesh Ewald method. *J. Chem. Phys.* **1995**, *103*, 8577–8593.
- (36) Kutzner, C.; Van Der Spoel, D.; Fechner, M.; Lindahl, E.; Schmitt, U. W.; De Groot, B. L.; Grubmüller, H. Speeding up parallel GROMACS on high-latency networks. *J. Comput. Chem.* **2007**, 28, 2075–2084.
- (37) Ryckaert, J.-P.; Ciccotti, G.; Berendsen, H. J. Numerical integration of the cartesian equations of motion of a system with constraints: molecular dynamics of n-alkanes. *J. Comput. Chem.* **1977**, 23, 327–341.
- (38) Miyamoto, S.; Kollman, P. A. Settle: An analytical version of the SHAKE and RATTLE algorithm for rigid water models. *J. Comput. Chem.* **1992**, *13*, 952–962.
- (39) Martyna, G. J.; Tobias, D. J.; Klein, M. L. Constant pressure molecular dynamics algorithms. *J. Chem. Phys.* **1994**, *101*, 4177–4189.
- (40) Feller, S. E.; Zhang, Y.; Pastor, R. W.; Brooks, B. R. Constant pressure molecular dynamics simulation: The Langevin piston method. *J. Chem. Phys.* **1995**, *103*, 4613–4621.
- (41) Machado, M. R.; Barrera, E. E.; Klein, F.; Sóñora, M.; Silva, S.; Pantano, S. The SIRAH 2.0 Force Field: Altius, Fortius, Citius. *J. Chem. Theory Comput.* **2019**, *15*, 2719–2733.
- (42) Abraham, M. J.; Murtola, T.; Schulz, R.; Páll, S.; Smith, J. C.; Hess, B.; Lindahl, E. GROMACS: High performance molecular simulations through multi-level parallelism from laptops to supercomputers. *SoftwareX* **2015**, *1*–2, 19–25.

- (43) Páll, S.; Abraham, M. J.; Kutzner, C.; Hess, B.; Lindahl, E. Tackling Exascale Software Challenges in Molecular Dynamics Simulations with GROMACS. Solving Software Challenges for Exascale. Cham 2015, 8759, 3–27.
- (44) Darré, L.; Machado, M. R.; Dans, P. D.; Herrera, F. E.; Pantano, S. Another Coarse Grain Model for Aqueous Solvation: WAT FOUR? *J. Chem. Theory Comput.* **2010**, *6*, 3793–3807.
- (45) Hockney, R.; Goel, S.; Eastwood, J. Quiet high-resolution computer models of a plasma. *J. Comput. Phys.* **1974**, *14*, 148–158.
- (46) Bussi, G.; Donadio, D.; Parrinello, M. Canonical sampling through velocity rescaling. *J. Chem. Phys.* **2007**, *126*, 014101.
- (47) Parrinello, M.; Rahman, A. Polymorphic transitions in single crystals: A new molecular dynamics method. *J. Appl. Phys.* **1981**, *52*, 7182–7190.
- (48) Benson, N. C.; Daggett, V. A chemical group graph representation for efficient high-throughput analysis of atomistic protein simulations. *J. Bioinform. Comput. Biol.* **2012**, *10*, 1250008.
- (49) R Core Team. R: A Language and Environment for Statistical Computing; R Foundation for Statistical Computing: Vienna, Austria, 2021
- (50) Butts, C. T. Social Network Analysis with sna. J. Stat. Software 2008, 24, 1–51.
- (51) Stone, J. An Efficient Library for Parallel Ray Tracing and Animation. M.Sc. Thesis, Computer Science Department, University of Missouri-Rolla, 1998.
- (52) Hurst, P. J.; Mulvey, J. T.; Bone, R. A.; Selmani, S.; Hudson, R. F.; Guan, Z.; Green, J. R.; Patterson, J. P. CryoEM Reveals the Evolution of a Thermodynamically Unstable Phase in the Chemical-Fueled Dissipative Assembly of a Disulfide Hydrogel. *Chem. Sci.*, **2023**. Manuscript in review.

□ Recommended by ACS

Stimulus-Induced Relief of Intentionally Incorporated Frustration Drives Refolding of a Water-Soluble Biomimetic Foldamer

Hanne C. Henriksen, Marcey L. Waters, et al.

DECEMBER 06, 2023

JOURNAL OF THE AMERICAN CHEMICAL SOCIETY

READ 🗹

Noncovalent Peptide Assembly Enables Crystalline, Permutable, and Reactive Thiol Frameworks

Selina S. Hess, Andy I. Nguyen, et al.

AUGUST 28, 2023

JOURNAL OF THE AMERICAN CHEMICAL SOCIETY

READ 🗹

Solution-based Supramolecular Hierarchical Assembly of Frenkel Excitonic Nanotubes Driven by Gold Nanoparticle Formation and Temperature

Seda Kelestemur, Dorthe M. Eisele, et al.

DECEMBER 29, 2023

THE JOURNAL OF PHYSICAL CHEMISTRY B

READ 🗹

Tailoring Synthetic Polypeptide Design for Directed Fibril Superstructure Formation and Enhanced Hydrogel Properties

Tianjian Yang, Yao Lin, et al.

JANUARY 04, 2024

JOURNAL OF THE AMERICAN CHEMICAL SOCIETY

READ 🗹

Get More Suggestions >